Digital Discovery

ROYAL SOCIETY OF CHEMISTRY

PAPER

View Article Online
View Journal

Cite this: DOI: 10.1039/d5dd00407a

Hierarchical attention graph learning with LLM enhancement for molecular solubility prediction

Yangxin Fan, [a] Yinghui Wu, [a] Roger H. French, [b] Danny Perez, [c] Michael G. Taylor [c] and Ping Yang *[c]

Solubility quantifies the concentration of a molecule that can dissolve in a given solvent. Accurate prediction of solubility is essential for optimizing drug efficacy, improving chemical and separation processes, and waste management, among many other industrial and research applications. Predicting solubility from first principles remains a complex and computationally intensive physicochemical challenge. Recent successes of graph neural networks for molecular learning tasks inspire us to develop HASolGNN, a hierarchical–attention graph neural network for solubility prediction. (1) HASolGNN adopts a three-level hierarchical attention framework to leverage atom-bond, molecular, and interaction-graph level features. This allows a more comprehensive modeling of both intra-molecular and inter-molecular interactions for solute–solvent dissolution as a complex system. (2) To mitigate the impact of small amounts of annotated data, we also investigate the role of Large Language Models (LLMs), and introduce HASolGNN-LLMs, an LLM-enhanced predictive framework that leverages LLMs to infer annotated features and embeddings to improve representation learning. Our experiments verified that (1) HASolGNN outperforms the state-of-the-art methods in solubility prediction; and (2) HASolGNN-LLMs effectively exploits LLMs to enhance sparsely annotated data and further improves overall accuracy.

Received 12th September 2025
Accepted 11th December 2025

DOI: 10.1039/d5dd00407a

rsc.li/digitaldiscovery

1 Introduction

Solubility is broadly relevant to many applications, including nuclear waste separation,[1,2] environmental pollution control,[3] development of advanced materials in the semi-conductor industry,[4,5] autonomous robotics synthesis,[6,7] crystallization,[8] and protein ligand bonding in the biomedical field.[9,10] In particular, aqueous solubility refers to the solubility of a solute in water. It plays an essential role in pharmaceutical science,[11–13] since (1) accurate prediction of solubility is critical for selecting promising drug candidates during the screening process, and (2) all drugs in the body exert their therapeutic effects in the form of aqueous solutions, which means lower solubility diminishes both their efficacy and bioavailability. Therefore, high-precision computational methods for solubility prediction can substantially decrease the experimental costs and time associated with drug development[14] while enabling chemists to develop formulations that maximize drug efficacy and improve patient outcomes.

Fig. 1 shows a solubility prediction pipeline, involving four components: solubility dataset curation, description generation, model training, and solubility prediction. Solubility data typically refer to the SMILES[15] of solute and solvent pairs, log S (log-scale solubility), as well as the molecular features such as melting point (MP), molecular weight (MW), and volume. The pipeline then converts the SMILES into (1) molecular graphs and (2) molecular fingerprints (physiochemical features). Molecular graphs will be used to train graph neural networks (GNNs) and their variants (*e.g.*, ref. 16–19), while molecular fingerprints are typically used by traditional machine learning and domain methods (*e.g.*, ref. 20–23). Next, the models predict solubility for critical applications in areas such as drug discovery.

1.1 State-of-the-art

Solubility prediction has been a long-standing challenge. A host of methods have been developed to predict the solubility of molecular systems. Recent approaches fall into three categories: (1) domain-specific methods, rooted in principles of quantum mechanics and thermodynamics; (2) traditional ML-based methods, which leverage established regression models and ensemble learning to predict solubility; and more recently, (3) graph neural network (GNN)-based methods, which utilize molecular graphs to model atoms and bonds and train GNNs as regression or classifiers.

(1) Domain-specific methods adhere to the quantitative structure–property relationship (QSPR) framework.[24] They regress solubility against a selected set of molecular descriptors, capturing

[a]Department of Computer Science, Case Western Reserve University, Cleveland, OH, USA. E-mail: yxf451@case.edu; yxw1650@case.edu

[b]Department of Material Science, Case Western Reserve University, Cleveland, OH, USA. E-mail: rxf131@case.edu

[c]Theoretical Division, Los Alamos National Laboratory, Los Alamos, NM, USA. E-mail: danny_perez@lanl.gov; mgt16@lanl.gov; pyang@lanl.gov

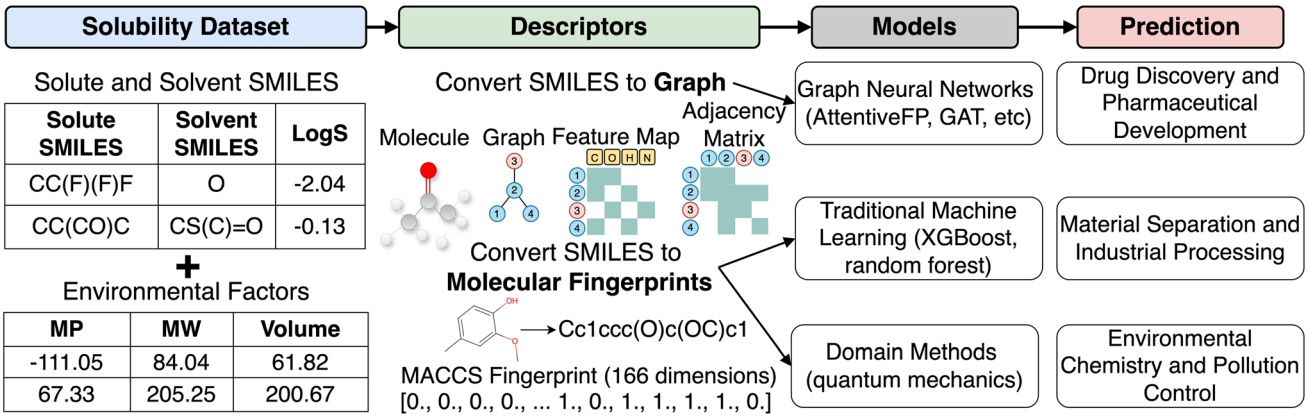

Fig. 1 Solubility prediction pipeline. Solubility prediction models are categorized into three major types, with critical applications spanning fields such as material separation and drug discovery.

the structural and physicochemical properties of compounds. Depending on the underlying theoretical foundation, such methods employ a range of mathematical models, including differential and partial differential equations, to predict solubility.[22,23,25]

(2) Among ML-based methods, boosting methods such as XGBoost[20] and random forest[21] have been widely applied. Other ML models include multi-layer perceptron (MLP)[26] and artificial neural networks (ANNs).[27,28] These methods take molecular fingerprints as input features, leveraging the encoded molecular-level structural information to predict solubility.

(3) Several GNN-based methods were developed, which exploit graph convolutional networks (GCNs),[16,17] gated graph neural networks (GGNNs),[29,30] node-level attention-based graph attention networks (GATs),[31,32] and molecular representation learning integrating both node- and graph-level attention mechanisms (AttentiveFP).[18,33] Among these methods, AttentiveFP has demonstrated superior performance, establishing itself as the current leading approach in GNN-based solubility prediction.[18]

Apart from the methods specifically developed for solubility prediction, recent studies have extended graph neural networks to related molecular property prediction tasks. Leenhouts *et al.*[34] introduced SolProp-mix, a GNN-based framework for predicting solvation free energy and enthalpy in solvent mixtures. Building on previous D-MPNN models for pure solvents, they proposed a permutation-invariant pooling function (MolPool) that enables learning across mixtures of arbitrary composition. Similarly, Jung *et al.*[35] developed a GNN framework to predict solubility in multicomponent solvent systems. They compared two GNN architectures: a concatenation model *versus* a subgraph model, with the latter showing higher accuracy by better capturing solute–solvent interactions. They incorporated a teacher–student semi-supervised distillation (SSD) approach to expand chemical coverage and improve prediction robustness.

1.2 Challenges & opportunities

While the aforementioned approaches have been applied for solubility prediction, several data challenges, and hence opportunities for improvement, remain.

(1) Rich features, "small" annotated data. Most methods fit models on molecular fingerprints alone. Sequential encoding often overlooks high-value features at the atom and bond ("edges" between atoms), and topological features at the molecular level. On the other hand, such features may be scarce in small and heterogeneous sources, among which few are annotated or labeled.

(2) Inter-molecular interaction: solubility is determined by a dynamic interaction process involving solute and solvent pairs. Existing GNN-based methods often model the solubility with atom- and bond-level representations of the solute alone, but lack the necessary expressiveness to explicitly and holistically characterize the dynamic interactions of solute–solvent pairs, and hence often hardly generalize for accurate solubility analysis.

(3) Existing domain-specific methods are often constrained by domain hypotheses and models, mostly leading to case-by-case analysis. Most methods are specialized for aqueous solubility or limited to fixed groups of solvents. Hence existing methods are often hard to be generalized for solubility prediction.

In response, we advocate the development of a solubility predictive framework as a "general recipe" to be broadly applied across diverse solute–solvent systems. Such a framework should be able to (a) best harvest a "hierarchy" of features from atom-, bond-, and molecular-level features, as well as environmental and other external features; (b) characterize inter-molecular interaction for more comprehensive and accurate modeling of solubility; and (c) easily integrate, annotate and align heterogeneous features with few or no annotated data.

1.3 Contribution

To address these challenges, we propose HASolGNN, a physics-informed graph model for solvent analysis.

(1) We propose HASolGNN, an expressive framework that can capture hierarchical, multi-level interactions and patterns among atom, bond, and (inter- and intra-) molecular features. HASolGNN enables solubility prediction across a wide range of solute–solvent pairs, irrespective of solvent types. HASolGNN achieves this through the integration of hierarchical attention mechanisms across three key components: the atom

embedding (AE) block, the molecular embedding (ME) block, and the interaction-graph embedding (IE) block. Experimental results demonstrate that HASolGNN significantly outperforms the state-of-the-art graph neural network methods, establishing new benchmarks in performance.

(2) We further propose HASolGNN-LLMs that integrates large-language models (LLMs) as a modular component, leveraging contrastive learning for fusion with HASolGNN to address the "small dataset" challenges frequently encountered by the scientific community. Our experiments show that HASolGNN-LLMs yields substantial improvements in solubility prediction under such data-scarce conditions, offering a potential solution to this common limitation.

(3) We conduct a new comprehensive evaluation of the performance of diverse graph neural network variants on three extensive and representative public solubility datasets, benchmarking our method's performance against the state-of-the-art methods. Our efforts offer valuable insights into the use of GNNs for solubility prediction that benefit both the chemistry and computer science communities.

We summarize other related work below.

1.4 Graph learning for system-level regression

Graph Neural Networks (GNNs)[36] have been extensively studied for general graph analysis tasks. A GNN may exploit spectral-based, attention-based, and spatial-based convolutions to manipulate node features, edge features, and graph-level representations. Notable variants include graph convolutional networks (GCNs),[37] GraphSAGE,[38] graph attention networks (GATs),[39] and graph isomorphic networks (GINs).[40] While GNNs are widely adopted for node classification or link prediction, the use of GNNs for system modeling with multiple participating molecules has been much less explored. As aforementioned, existing GNN-based methods, while being adaptable for graph-based molecular property prediction, rely on graph-level pooling strategies to produce numeric predictions for solubility. Therefore, these approaches overlook the potentially complex interactions among molecules, as they remain constrained to explicitly model the interactions among molecules in a dynamic system.

1.5 Graph learning for molecular property prediction

Recent effort has applied graph learning for molecular property prediction. Recurrent graph neural networks (RGNNs)[41–45] were among the first GNNs utilized for molecular property prediction. RGNNs iteratively apply shared weight matrices, enabling the model to capture dependencies over multiple iterations. Conv-GNNs[46–50] introduce iteration-specific weights, enhancing flexibility and expressiveness. Specifically, spectral Conv-GNNs operate in the spectral domain using graph Laplacian transformations, while spatial Conv-GNNs directly aggregate features from neighboring nodes. Architectural innovations such as advance pooling strategies,[51,52] skip-connections,[53,54] and architecturally distinct GNNs[55,56] can be integrated into GNNs in general to improve feature aggregation for molecular system modeling. We consider these as potential opportunities to improve our methods in the future.

2 Methods

2.1 Preliminary

2.1.1 Molecule as a graph. We represent a molecule as a graph $G = (V, E, X, Y, \mathscr{F})$, where V is a node set, in which each node represents an atom; and E refers to the set of edges (bonds) between atoms. X is a node feature matrix, where each entry x_u represents the node feature vector of node $v \in V$. The node feature vector includes atomic number, degree (number of bonds connected to the atom), formal charge, number of unpaired electrons (radical electrons), hybridization state (*e.g.*, sp^3, sp^2, and sp), aromaticity, number of implicit hydrogen atoms, chirality and chirality type.[19]

Similarly, Y is a bond feature matrix, where for each edge (bond) $e \in E$, Y_e is a feature vector that contains bond type (single, double, triple, or aromatic), conjugation (binary, 1 if the bond is conjugated, 0 otherwise), ring (1 if the bond is part of a ring, 0 otherwise), and stereo (a one-hot encoded vector of length 4 to represent the stereochemistry of the bond).[57]

In addition, $\mathscr{F}$ contains graph-level features, encompassing structural and functional characteristics (*e.g.* molecular weight and total charge), along with environmental factors such as temperature and pH, which influence the molecule's behavior.

2.1.2 Molecule system regression. We define molecule system regression as a class of tasks on predicting properties arising from complicated interactions among p molecules. Given a series of molecular graphs G_1, G_2, …, G_p, and historical data of their (chemical) reactions, it aims to derive a regression model to predict a numeric value for system-level computable properties, such as solubility, affinity, toxicity, and side effects.

Solubility prediction is a special case of the above system-level regression problem when $p = 2$, specifying two interacting classes of molecules: the solute (G_1) and the solvent (G_2). Our goal is to train a GNN model M, which takes G_1 and G_2 as input to minimize solubility prediction errors $\mathscr{L}_S(G_1, G_2, L, \theta)$, where L and θ refer to ground-truths and the set of parameters in M, respectively.

Conventional GNNs fall short of directly serving as a desired model M due to limited expressiveness. Ideally, (1) M should be able to exploit the rich features from different levels in G_1 and G_2, ranging from atom-level to molecule-level; (2) M should be expressive enough to describe the physical nature of solubility as an interactive system, which not only capture molecule-level embeddings, but also capture complex atomic and bond interactions, as well as the "non-local" interactions among the molecules. This allows explicit modeling of the molecular interactions between the solute and the solvent pairs, beyond what a straightforward application of GNNs can express.

2.2 HASolGNN framework

We next introduce the HASolGNN architecture and its key components including the input layer, atom embedding block, molecular embedding block, and interaction-graph embedding block.

2.2.1 Model architecture. We start with the architecture of HASolGNN, as illustrated in Fig. 2. It consists of the following key modules.

2.2.1.1 Featurization and input layer. HASolGNN converts the SMILES representations of solute S_1 and solvent S_2 into the featurized solute graph $G_1 = (V_1, E_1, X_1, Y_1, \mathscr{F}_1)$ and solvent graph $G_2 = (V_2, E_2, X_2, Y_2, \mathscr{F}_2)$. The input layer standardizes them into $\hat{G}_1$ and $\hat{G}_2$ by combining their node and bond features;

2.2.1.2 Molecular fingerprint generation module (MFGM). HASolGNN fits $\hat{G}_1$ and $\hat{G}_2$ into MFGMs. Each MFGM is composed of one Atom Embedding (AE) block and two Molecule Embedding (ME) blocks. The AE block processes G_1 or G_2, while the ME blocks take G_1M or ${G_2}^M$ as input. Here, ${G_1}^M$ (resp. ${G_2}^M$) refines its original counterpart G_1 (resp. G_2) with a simple "star-structure", each containing a centering "supernode" connected to all the atoms in G_1 or G_2. The embeddings produced by the AE block are fed into the first ME block. In contrast, the second ME block directly utilizes the initial node and bond features of the molecular graphs;

2.2.1.3 Embedding fusion. HASolGNN leverages a novel fusion mechanism to combine the embeddings representing molecule level representations of the solute and solvent from the two MFGMs with graph-level features $\mathscr{F}_1$ and $\mathscr{F}_2$ to generate the molecular fingerprints $\mathrm{MF}_{\mathrm{solute}}$ for the solute and $\mathrm{MF}_{\mathrm{solvent}}$ for the solvent;

2.2.1.4 Interaction graph. HASolGNN constructs the interaction graph comprising two nodes: G_1, representing the solute with $\mathrm{MF}_{\mathrm{solute}}$ as its node features, and G_2, representing the solvent with $\mathrm{MF}_{\mathrm{solvent}}$ as its node features. The integration-graph embedding (IE) block processes the interaction graph to produce the system-level fingerprint $\mathrm{MF}_{\mathrm{IG}}$, which is passed to the output layer to predict solubility (Fig. 3).

We next detail the key components of HASolGNN.

2.2.2 Input layer. For each node $v \in V$, the input layer concatenates the node features from the neighboring nodes and edge features from the incident edges and unifies the node representations across all nodes by taking both initial atom and bond features into account. The input layer standardizes the input and ensures that both the initial bond and atom features participate in the following message passing. The input layer generates the updated molecular graphs, incorporating enhanced node features derived from the original node and edge attributes. These updated graphs $\hat{G}_1$ and $\hat{G}_2$ are then passed to the downstream AE block and one of the ME blocks in the MFGM. Formally, we represent the input layer as follows:

$$
\begin{aligned}
{h_v}^0 &= \mathrm{ReLU}\left(W_{fc_1} x_v\right), \quad \forall v \in V; \\
{h_u}^0 &= \mathrm{ReLU}\left(W_{fc_2}\mathrm{CONCAT}(x_u, y_{vu})\right), \quad \forall u \in N(v); \\
{a_{vu}}^0 &= \mathrm{Soft\,max}\left(\mathrm{LeakyReLU}\left(W\left[{h_v}^0, {h_u}^0\right]\right)\right); \\
{h_v}^1 &= \mathrm{GRU}\left(\mathrm{ELU}\left(\sum_{u \in N(v)} a_{vu} W {h_v}^0\right), {h_v}^0\right)
\end{aligned}
\tag{1}
$$

where W_{fc_1}, W_{fc_2}, and W are learnable weight matrices, and ELU denotes the exponential linear unit activation function.

2.2.3 Atom Embedding (AE) block. As illustrated in Fig. 5, the atom embedding (AE) block consists of an iterative process comprising (1) a message-passing phase, implemented using a Graph Attention Network (GAT) layer, followed by (2) a readout phase utilizing a Long Short-Term Memory (LSTM) layer that performs information filtering and models long-range dependencies. The AE block fits directly on the output of the input layer $x_0 = h_1$, the updated node embedding derived by the input layer. At the first iteration, both the hidden state h_1 and cell state c_1 are initialized to x_0. At the t-th iteration ($t > 1$), h_t is

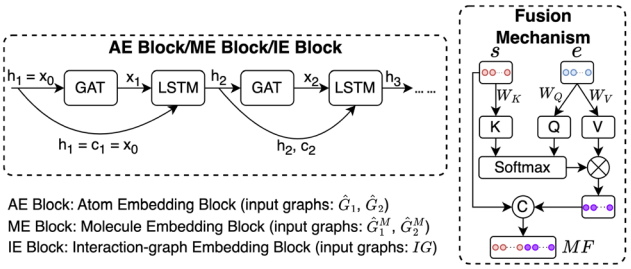

Fig. 3 Internals of the atom embedding block, molecule embedding block, and interaction-graph embedding block (a series of GAT and LSTM layers) and the fusion mechanism (fusion of graph-level structural representations and environmental factors).

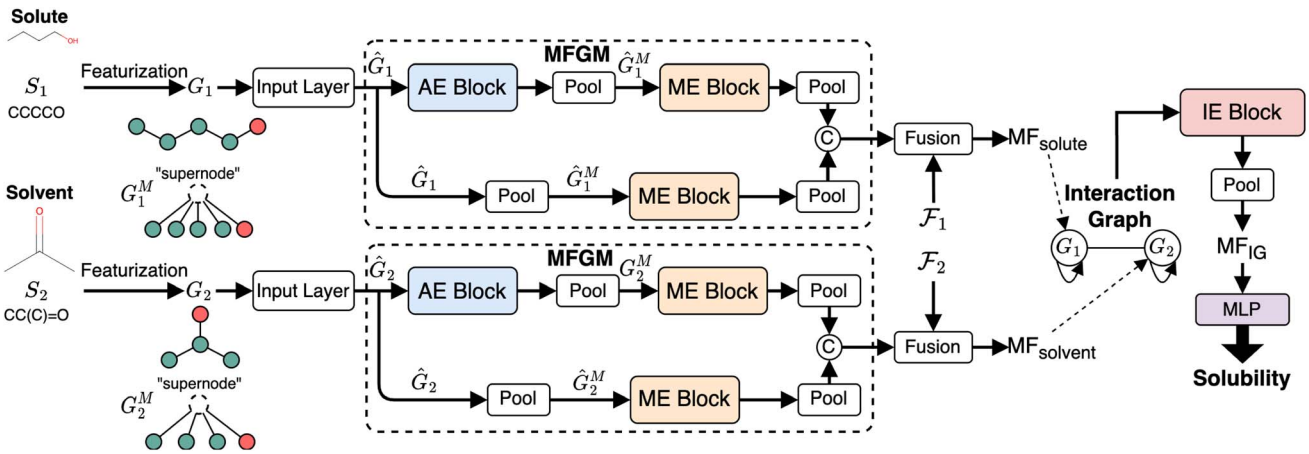

Fig. 2 HASolGNN framework. MFGM: molecular fingerprint generation module. Molecular graphs G_1 of the solute and G_2 of the solvent are fitted into different MFGMs, each consisting of one AE block and two ME blocks. The IE block fits on the interaction graph and outputs the system-level representation. $\mathrm{MF}_{\mathrm{IG}}$ is fitted into the output layer to generate solubility prediction.

passed to the t-th GAT layer to compute x_t, which serves as the input to the t-th LSTM layer. The t-th LSTM layer updates its hidden state to h_{t+1} and cell state to c_{t+1}. We represent the iterative refinement process as follows:

$$(h_{t+1},c_{t+1}) = \mathrm{LSTM}(\mathrm{GAT}(h_t,A_G),(h_t,c_t)),\ t\in[1,k] \quad (2)$$

After the k-th iteration, the final hidden state h_{k+1} will be forwarded to the downstream tasks.

2.2.4 Molecular Embedding (ME) block. Within each MFGM, two ME blocks that process synthetic graphs with identical topology, where a single supernode connects to all atoms in the molecular graph. However, the node features differ between these blocks. For the top ME block, node features are computed from the output of the AE block such that (1) the initial supernode embedding is obtained by pooling h_{k+1} and (2) the node features of all atoms are directly inherited from the their embeddings in h_{k+1}. In contrast, the bottom ME block constructs node features from the output of the input layer such that (1) the initial supernode embedding is derived by pooling h^1 and (2) the node features of all atoms directly inherited from the updated molecular graphs from the input layers (Fig. 4).

2.2.5 Fusion mechanism. We propose a novel fusion mechanism to integrate graph-level features $\mathscr{F}_1$ and $\mathscr{F}_2$ that capture contextual information such as environmental factors (EFs) with the embeddings from the output of the MFGM, which convey structural relationships. Our fusion mechanism, illustrated in Fig. 5, comprises two steps: (1) cross-attention and (2) concatenation.

The cross-attention module consists of learnable parameters: query W_Q, key W_K, and value W_V. These are used to compute the cross-attention scores between the structural GNN embeddings and the EFs. Specifically, it calculates the cross-attention score between the molecule-level structural representation s obtained from the MFGM and the environmental factors vector e defined in Sec. 2, where s serves as the key, representing the referenced information. The resulting attention weight α transforms e into e', which will be then concatenated with s to derive the molecular fingerpints $\mathrm{MF}_{\mathrm{solute}}$ for the solute and $\mathrm{MF}_{\mathrm{solvent}}$ for the solvent. Formally, we represent the fusion mechanism as follows:

$$\alpha = \mathrm{Soft\ max}\left(\frac{\mathrm{QK}^{\mathrm{T}}}{\sqrt{d_{\mathrm{k}}}}\right); e' = \alpha V;$$
$$\mathrm{MF} = \mathrm{CONCAT}\left(s, e'\right) \quad (3)$$

where $Q = W_{\mathrm{Q}}e$, $K = W_{\mathrm{K}}s$, and $V = W_{\mathrm{V}}e$. The term d_{k} denotes the dimensionality of the key embeddings s.

2.2.6 Interaction-graph Embedding (IE) block. HASolGNN constructs the interaction by creating two interconnected nodes, each representing the solute and solvent, respectively. HASolGNN fuses the outputs of the two MFGMs with

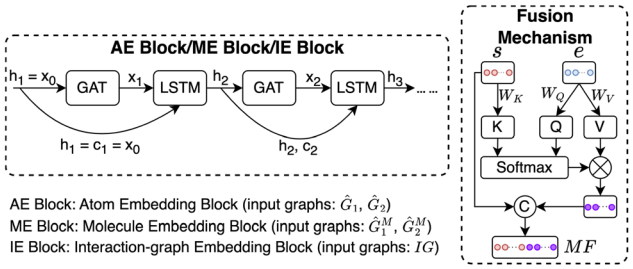

Fig. 5 Internals of the atom embedding block, molecule embedding block, and interaction-graph embedding block (a series of GAT and LSTM layers) and the fusion mechanism (fusion of graph-level structural representations and environmental factors).

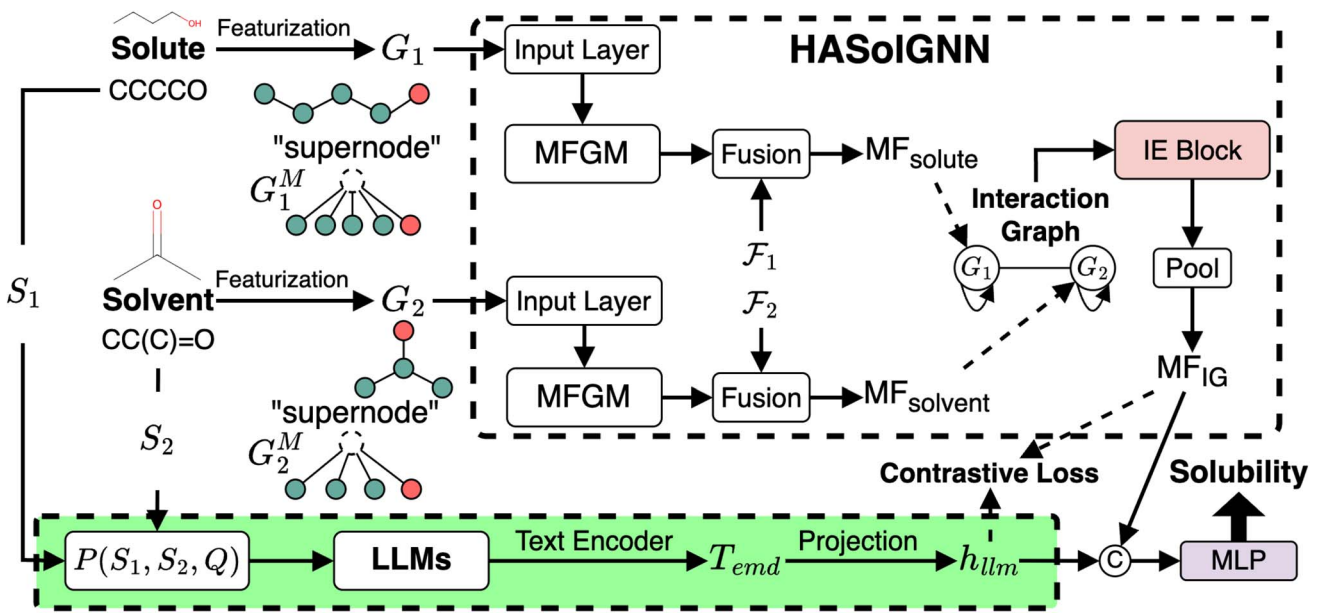

Fig. 4 HASolGNN-LLMs. The LLM module collaborates with HASolGNN to learn representations by aligning h_{llm} from GNNs and $\mathrm{MF}_{\mathrm{IG}}$ from LLMs within a shared embedding space. A contrastive loss $\mathscr{L}_{\mathrm{c}}$ enforces this alignment, ensuring that complementary knowledge can be effectively leveraged from both sources.

environmental factors (EFs) to derive the molecular fingerprint for the solute MF_{solute} and the molecular fingerprint of the solvent $MF_{solvent}$. These molecular fingerprints are assigned as the node features for their corresponding nodes. The IE block then processes the integration graph as the computation graph to compute the system-level fingerprint, MF_{IG}.

2.2.7 Hierarchical attention mechanism. HASolGNN employs GATs at every iteration of the message-passing phase within the AE, ME, and IE blocks, as well as the input layer. This design establishes a three-level hierarchical attention mechanism: (1) node-level and bond-level attentions to capture fine-grained features from the molecular graphs; (2) molecule-level attention derived from synthetic graphs, where each graph includes a supernode connected to all atoms in the corresponding molecular graph; and (3) system-level attention to extract high-level interactions from the interaction graph. HASolGNN leverages this hierarchical message-passing framework to encode information in a progressively compact manner, transforming detailed atom and bond features progressively into a compact and structured system-level representation.

2.2.8 Loss function. During model training, the set of parameters θ of the HASolGNN model M is optimized by minimizing the errors between the solubility prediction of HASolGNN and the ground-truth values:

$$\mathscr{L}_S(G_1, G_2, L, \theta) = \frac{1}{N}\sum_{i=1}^{N}\left(P_{M(G_1,G_2,\theta)}(i) - L(i)\right)^2 \quad (4)$$

where N represents the number of solute–solvent pairs in the training set, P_M denotes the predictions made by HASolGNN, and L corresponds to the ground-truth solubility values.

2.2.9 Cost analysis. The training complexity of HASolGNN is $O(ek|E|dF^2 + ek|V|F^2)$, and the inference cost is $O(k|E|dF^2 + k|V|F^2)$. Here, $|E| = |E_1| + |E_2|$ and $|V| = |V_1| + |V_2|$; e, k, F, and d refers to the number of epochs, number of iterations in the AE block, number of features per node, and the maximum node degree of G_1 and G_2, respectively. Please refer to the SI for a detailed analysis and proof.

2.3 LLM-enhanced HASolGNN

To mitigate the challenge posed by small datasets, we present HASolGNN-LLMs, an LLM-enhanced variant of HASolGNN. It leverages LLMs as (1) a feature enricher: expanding the feature space and enhancing molecular representations to maximize the utility of available context for solubility prediction from unstructured textual input such as lab, instrument or literature; and (2) a pseudo-annotator: providing estimations of solubility that are guided by proper prompting and conform to the context.

2.3.1 Architecture details. We next introduce the primary components of the pluggable LLM module integrated into HASolGNN-LLMs.

2.3.1.1 Generating textual descriptions. HASolGNN-LLMs incorporates a customizable library of LLMs, including, for example, GPT-4 (ref. 58) and Llama 3 (ref. 59), to generate textual descriptions of solubility estimations based on their structural and chemical properties of both solute and solvent molecules. Specifically, given a solute–solvent pair, we incorporate the SMILES strings of the solute S_1 and solvent S_2 to query LLMs with the following template $P(S_1, S_2, Q)$†:

> "Given two molecules represented by SMILES strings: Solute: [S_1]; Solvent: [S_2]. We also know [Q]). Using explicit molecular structures, provide precise, concise, and structure-based descriptions about the solubility of [S_1] in [S_2]. Discuss chemical properties mentioned in [Q] that influence solubility, such as polarity, hydrogen bonding, and molecular size. Avoid speculative physicochemical inferences."

Here Q refers to user-specified, task-specific domain knowledge such as knowledge about the chemical structure.[10,61] In practice, Q consists of curated documents that outline key factors influencing solubility, include illustrative examples and contain answers from relevant literature. This ensures that the generated descriptions are grounded in established chemical knowledge.

2.3.1.2 Deriving the embedding h_{llm}. Upon the generation of textual descriptions by LLMs, HASolGNN-LLMs utilizes a text encoder such as SciBERT[62] and PubmedBERT[63] to transform chemical textual descriptions into global-level text embeddings T_{emd} by extracting the [CLS][62] token embedding. Given the high dimensionality of T_{emd}, HASolGNN-LLMs employs a multi-layer perceptron (MLP) to project T_{emd} into a low-dimensionality latent space, h_{llm}, aligning its dimensionality with that of the MF_{IG} to ensure compatibility. In the case of SciBERT, we specify the process as follows:

$$h_{llm} = \mathrm{MLP}(\mathrm{SciBERT}(\mathrm{LLMs}(P(S_1,S_2,Q)))) \quad (5)$$

2.3.1.3 Embedding enhancement. To integrate the embeddings from HASolGNN with the LLM module effectively, HASolGNN-LLMs learns a joint representation by combining the system-level HASolGNN embeddings MF_{IG} with the textual embeddings h_{llm} derived from the LLM module. We employ an unsupervised contrastive loss, L_c (please refer to Eqn. (6)), to minimize the distance between MF_{IG} and h_{llm} for the same solute–solvent pair. Besides, we incorporate a negative sampling strategy[64] to construct negative solute–solvent pairs (τ, τ'), where $\tau = (S_1, S_2)$ and $\tau' = (S_1', S_2')$ such that $\tau \neq \tau'$. For these negative pairs, L_c maximizes the distance (minimizes the similarity) between MF_{IG} of τ and h_{llm} of τ', ensuring proper separation between positive and negative pairs. This allows HASolGNN-LLMs to differentiate between positive and negative pairs, improving its predictive and representational capabilities.

2.3.1.4 Loss Function. The loss function of HASolGNN-LLMs $\mathscr{L}$ comprises (1) a supervised $\mathscr{L}_s$ that captures the solubility prediction errors from HASolGNN and (2) an unsupervised contrastive loss $\mathscr{L}_c$ to ensure the proper enhancement by combing the system-level MF_{IG} from HASolGNN and the projected h_{llm} derived from the LLM module. We formulate $\mathscr{L}$ as follows:

† We showcase example prompts and LLM responses in the full version.[60]

"I have two molecules represented by SMILES strings: Solute: [CCO]; Solvent: [O]. Based on their **molecular structures**, provide specific, compact, and tailored descriptions about the **solubility** of the solute in the solvent. Discuss any **chemical properties** that influence solubility, such as **polarity**, **hydrogen bonding**, **molecular size**, or others. "

Fig. 6 An example of the prompt used to query the LLM.

$$\begin{aligned}\mathscr{L}(G_1, G_2, L, \theta, S_1, S_2, Q) &= \mathscr{L}_{\mathrm{S}}(G_1, G_2, L, \theta) \\ &\quad + \lambda \mathscr{L}_{\mathrm{c}}(\mathrm{MF}_{\mathrm{IG}}(G_1, G_2, \theta), h_{\mathrm{llm}}(S_1, S_2, Q)); \\ \mathscr{L}_{\mathrm{c}} &= \frac{1}{2N}\sum_{i=1}^{N}\left[y_i \cdot D_i^2 + (1-y_i)\cdot \max(0, m - \mathrm{D}_i)^2\right]\end{aligned} \tag{6}$$

Here, D_i is the distance equal to one minus the similarity between the i-th $\mathrm{MF}_{\mathrm{IG}}$ and i-th h_{llm}, m is a margin value, λ denotes the balancing factor between $\mathscr{L}_{\mathrm{S}}$ and $\mathscr{L}_{\mathrm{c}}$, and y_i indicates whether the pair is positive ($y_i = 1$) or negative ($y_i = 0$).

2.3.2 An example of the prompt and LLM response. We showcase an example of the prompt following the template $P(S_1, S_2, Q)$ and its corresponding response from the LLM. Fig. 6 illustrates an example of the prompt for querying the solubility of solute [CCO] in solvent [O]. Fig. 8 provides the corresponding response from GPT -4 for the above prompt. We highlight the key words in different colors and their corresponding responses in same color.

How LLMs help the small-data challenge? The LLM component in HASolGNN-LLMs is designed to address the small-data limitation by infusing domain knowledge and generating complementary representations that go beyond what can be learned from limited labeled samples. Specifically, LLMs act as both a feature enricher and a pseudo-annotator. (1) As a feature enricher, the LLM leverages its pretrained knowledge of chemical language and concepts to produce detailed, structure-aware textual descriptions of solute–solvent pairs, which are then encoded into dense embeddings. These embeddings enrich the molecular feature space with contextual chemical information that may not be directly observable from graph structures alone. (2) As a pseudo-annotator, the LLM provides approximate solubility estimations through guided prompting, effectively augmenting supervision in low-data regimes. By aligning these LLM-derived embeddings with the graph-based representations using a contrastive loss,

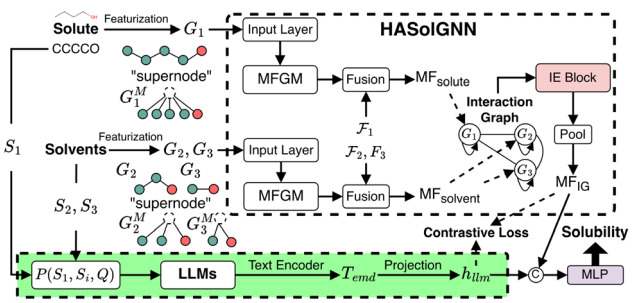

Fig. 7 Adapted variant of HASolGNN-LLMs with cosolvents G_2 and G_3.

"The solute is represented by the SMILES string "CCO", which corresponds to the chemical structure of ethanol. Ethanol is a two-carbon alcohol, with a hydroxyl (-OH) functional group attached to one of the carbon atoms. The solvent is represented by the SMILES string "O", which corresponds to the chemical structure of water. Water is a polar molecule with two hydrogen atoms bonded to one oxygen atom. The solubility of a solute in a solvent is largely determined by the "like dissolves like" principle, which states that polar solutes dissolve in polar solvents, and nonpolar solutes dissolve in nonpolar solvents. Both ethanol and water are polar molecules, so we would expect ethanol to be soluble in water. Ethanol is polar because of the -OH group, which has a polar bond due to the difference in electronegativity between oxygen and hydrogen. This allows ethanol to form hydrogen bonds with water, further enhancing its solubility. The two carbon atoms in ethanol contribute some nonpolar character to the molecule, but this is not enough to prevent it from dissolving in water. In terms of molecular size, ethanol is a relatively small molecule, which also favors solubility in water. Larger molecules tend to have more nonpolar character and are therefore less soluble in polar solvents. In conclusion, based on the polarity, ability to form hydrogen bonds, and small size of ethanol, we would expect it to be **highly soluble** in water."

Fig. 8 Response from GPT-4 for the prompt in Fig. 6.

HASolGNN-LLMs learns to transfer chemically relevant patterns from the LLM's large-scale pretraining to the solubility prediction task, thereby improving generalization and robustness despite the small dataset size.

2.3.3 Extension of HASolGNN-LLMs to other reactions. HASolGNN-LLMs can be adapted to handle more critical reactions such as co-solvents, counter-ions, and (de-)protonation reactions. For example, Fig. 7 illustrates a variant of HASolGNN-LLMs that takes a pair of solvents as the input instead of just one solvent. Note that, in this case, there are three nodes in the interaction graph where two denote solvents and one represents solute. Currently, the factors highlighted by the referee (co-solvents, counter-ions, and (de-)protonation reactions) are not reported in the datasets that we considered. Therefore, data availability is a critical consideration in extending these models towards more complex chemical spaces.

3 Results and discussion

We experimentally evaluate the performance of HASolGNN, comparing it with ten GNN baseline models. Moreover, we evaluate the performance of HASolGNN-LLMs to understand whether or how LLMs may be exploited. Our source code, datasets, and a full version of the paper are made available ‡.

3.1 Methods

3.1.1 Evaluation metrics. We evaluate the performance of our solubility predictions and baselines using Mean Absolute Error (MAE) and R-squared, where solubility predictions by

‡ https://github.com/Yangxin666/HASolGNN

HASolGNN, HASolGNN-LLMs, and all baselines are expressed as the natural logarithm (base e) of the solubility values.

3.1.2 Datasets. To validate the effectiveness of our model, we conduct experiments on three large-scale benchmark solubility datasets. We clarified the overlaps among the three curated datasets. Exp-DB contains the largest number of unique solute–solvent pairs, while MolMerger, which integrates data from BigSolDB, BNNLabs Solubility, and ESOL, exhibits substantial overlap with BigSolDB (overlap size = 4964). In contrast, the direct overlaps between Exp-DB and BigSolDB, and MolMerger and Exp-DB are smaller (overlap size = 51 and 1189 respectively). To estimate dataset noise, we examined repeated solubility measurements (*e.g.,* identical solute–solvent pairs measured under similar conditions). The per-pair standard deviation across such duplicates indicates an intrinsic noise level of approximately 0.53 $\log S$ units on average across the three datasets, reflecting the experimental uncertainty inherent in solubility measurements. HASolGNN's test error (MAE $\approx$ 0.73 $\log S$ for Exp-DB and $\approx$ 0.75 $\log S$ for BigSolDB) is consistent with statistical limit, suggesting that the performance is noise-limited rather than model-limited, indicating that further improvements are constrained by data noise rather than by the expressiveness or capacity of HASolGNN.

(1) Exp-DB:[65] this dataset contains 11 637 experimentally measured solubility values at temperatures of 298 K ($\pm$2 K). Each value corresponds to a unique solute–solvent pair. It is the largest dataset in terms of unique pair counts. (2) MolMerger:[66] it comprises 6975 unique solute–solvent pairs, each with a measured solubility value at temperatures near 273 K. The MolMerger dataset integrates data from three distinct sources: 4964 values from BigSolDB,[15] 1093 values from BNNLabs Solubility,[67] and 972 values from ESOL.[68] (3) BigSolDB:[15] the largest solubility dataset in terms of sample sizes. It includes 54 273 individual solubility values for 830 unique molecules and 138 distinct solvents, measured over a temperature range of 243.15 to 403.15 K at atmospheric pressure. Despite its size, BigSolDB contains fewer unique solute–solvent pairs compared to the other two datasets, with only 4964 unique pairs.

For Exp-DB and MolMerger, no environmental features are reported. For BigSolDB, the only reported environmental feature is temperature.

We ensure that data splitting for all datasets is performed strictly based on unique solute–solvent pairs. In particular, BigSolDB contains multiple solubility measurements for identical solute–solvent pairs across varying temperatures. To prevent data leakage, we group all entries sharing the same solute–solvent pair as a single unit before performing the split. This guarantees that all temperature-dependent measurements of a given pair remain entirely within one subset (training, validation, or testing). For Exp-DB and MolMerger, we partitioned each dataset based on unique solute–solvent pairs, assigning 60% for training, 20% for validation, and 20% for testing to ensure fair and consistent performance evaluation. For BigSolDB, because solute–solvent pairs exhibit distinct temperature ranges, we adopted a slightly adjusted split of 62.2% for training, 18.5% for validation, and 19.3% for testing to maintain balanced coverage across temperature conditions.

3.1.3 Baselines. We compare HASolGNN with following baselines: (1) GCN:[16] applies a localized first-order approximation of spectral graph convolutions; (2) GAT:[31] graph attention networks with a node-level attention mechanism, using self-attention to learn the attention scores for the neighbors; (3) GraphSAGE:[69] learns node embeddings by sampling and aggregating features from a node's local neighborhood; (4) GIN:[18] graph isomorphic network aggregates node features using a sum function, followed by a MLP to update embeddings. It is provably as powerful as the Weisfeiler Lehman graph isomorphism test. (5) GatedGNN:[29] uses gated recurrent units (GRUs) to propagate information across nodes in a graph over multiple time steps, enabling the network to capture complex dependencies; (6) ResGatedGNN:[29] incorporates residual networks into multi-layer gated graph ConvNets. (7) CGCN:[70] Crystal Graph Convolutional Neural Network (CGCN) is a graph convolutional neural network framework to learn graph-level properties from the connection of nodes in the graph, providing a universal and interpretable graph-level representation. (8) GraphTransformer:[71] utilizes multi-head attention to enable attentive information propagation between nodes, enhancing graph learning capabilities. (9) MFGNN:[30] MFGNN

Table 1 Comparison of solubility prediction errors (MAE) for HASolGNN and baselines – best results in bold

Methods	Exp-DB	MolMerger	BigSolDB
GCN[16]	0.9911	0.9450	1.2926
GAT[31]	0.9538	0.8856	1.3035
GraphSAGE[69]	0.9971	0.9446	1.2851
GIN[18]	0.9519	0.9520	1.2691
GatedGNN[29]	0.9191	0.8518	1.2592
ResGatedGNN[29]	0.9606	0.8754	1.2830
CGCN[70]	1.0184	0.9758	1.3534
GraphTransformer[71]	0.9452	0.9006	1.2737
MFGNN[30]	0.9542	0.8425	1.2695
AttentiveFP[33]	*0.8688*	*0.8036*	*1.0521*
XGBoost[72]	1.0293	0.9847	1.3858
MPFP[73]	0.9635	0.8702	1.2781
HASolGNN (ours)	**0.7315**	**0.7124**	**0.7408**
Improvements over AttentiveFP	15.81%	11.35%	29.59%

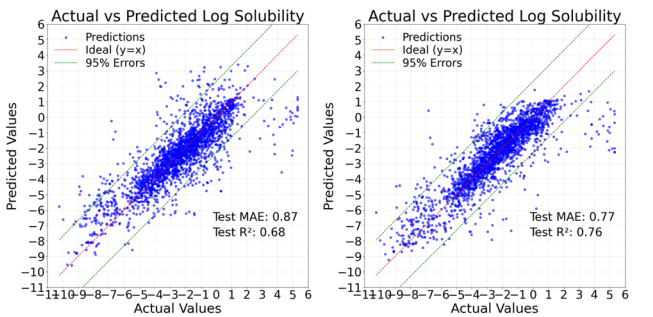

(a) AttentiveFP. (b) HASolGNN.

Fig. 9 Visualization of solubility prediction errors of HASolGNN *vs.* AttentiveFP on Exp-DB (MAE & R-squared).

introduces a GNN that allows end-to-end learning of prediction pipelines whose inputs are graphs of arbitrary size and shape. (10) AttentiveFP:[33] the SOTA GNN molecular representation learning method. AttentiveFP leverages both atom- and molecule-level attention mechanisms by stacking graph attention networks with gated-recurrent units to capture the hierarchical molecular structures. AttentiveFP is capable of extracting non-local intramolecular interactions that are intractable for other graph-based representations. (11) XGBoost,[72] an optimized gradient boosting framework based on decision trees, trained on hand-crafted molecular descriptors and fingerprints rather than graph-based representations. (12) MPFP:[73] message-passing with fingerprints implements a message-passing neural network (MPNN) using traditional circular fingerprints as node features, bridging the gap between classical molecular descriptors and learned representations.

We trained all baselines with consistent settings (data splits, hyperparameter tuning, *etc.*) for fair comparisons. Only AttentiveFP adopted a two-level (atom and molecular) representation. For the rest, we adopted, as a routine, the node-level features (SMILES).

3.1.4 Hyperparameter tuning. We perform a grid search over the validation loss to find the optimal set of hyperparameters, following the methodology outlined in ref. 74. We varied k of the AE block in the set {1, 2, 3, 4}, t of the ME block in the set {1, 2, 3, 4}, h of the IE block in the set {1, 2, 3, 4}, the number of epochs e in the set {25, 50, 100, 150, 200}, the learning rate lr from {0.001, 0.01, 0.05, 0.1}, the contrastive balancing term λ in the set {0.5, 1, 5, 10, 25, 50, 100}. Within GPT-4, we vary temperature in {0.1, 0.3, 0.5, 0.7, 0.9} and top_p in {0.1, 0.3, 0.5, 0.7, 0.9}. Based on the validation loss, we choose k equal to 3, t, h, and λ to be 3, 1, and 5, epochs to be 100, lr to be 0.01, temperature to be 0.3 and top_p to be 0.7.

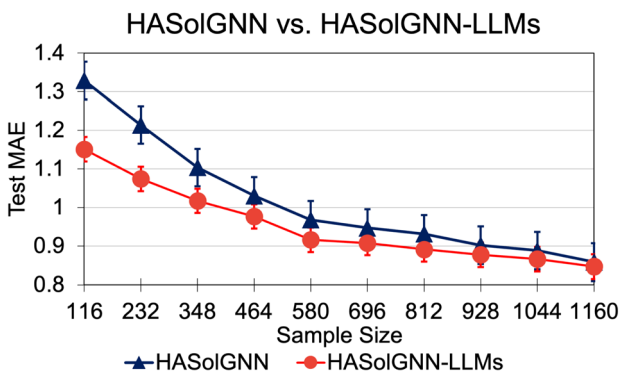

(a) Test MAE.

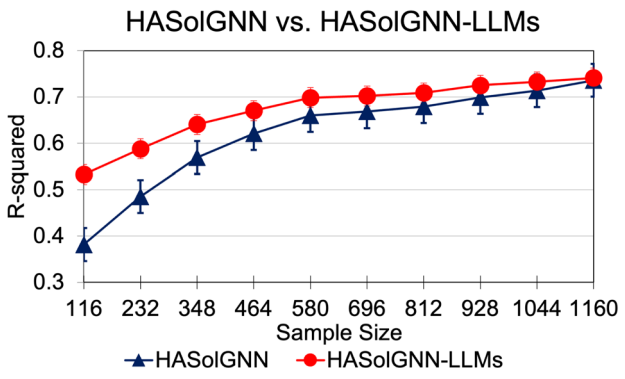

(b) Test R-squared.

Fig. 10 Test MAE and R-squared of HASolGNN *vs.* HASolGNN-LLMs on a small dataset. Sample sizes from 116 to 1160 correspond to 1–10% randomly sampled data from Exp-DB. The test MAE of each sample size is averaged from 50 different samples.

3.2 Results and discussion

3.2.1 Solubility prediction accuracy. We first report the performance of HASolGNN across all three datasets, compared to ten GNN baselines. As shown in Table 1, AttentiveFP achieves the best results across all baselines. HASolGNN outperforms AttentiveFP by further reducing MAE by 15.81%, 11.35%, and 29.59% on the Exp-DB, MolMerger, and BigSolDB dataset, respectively. Fig. 9 visualizes the solubility prediction errors of HASolGNN compared to AttentiveFP on Exp-DB. The results indicate that HASolGNN predictions align more closely with the ideal fit (where predicted values equal actual values). Specifically, compared to AttentiveFP, HASolGNN (1) achieves a lower test MAE and a higher test R-squared; (2) produces 29.92% (178 compared to 254) fewer predictions with absolute errors exceeding two (outside the two green lines). Next, we compare the performance of HASolGNN over non-GNN-based methods. XGBoost uses handcrafted molecular descriptors and therefore typically performs worse than GNNs, which learn molecular structures directly. MPFP adds learned propagation over fingerprint features and performs better than XGBoost, but below mid-tier GNNs (*e.g.*, GatedGNN, GIN).

How LLMs improve performance on "small" datasets? To study how the LLM module potentially improves the performance over the small dataset, we randomly sample subsets with sample size ranging from 116 to 1160, corresponding to 1% to 10% the size of the Exp-DB dataset. For each sample size, we randomly sample 50 different sample sets and calculate the average and standard deviation from them, as shown in Fig. 10. We follow the same training, validation, and test split proportions described in Sec. 3.1. We observe the followings from

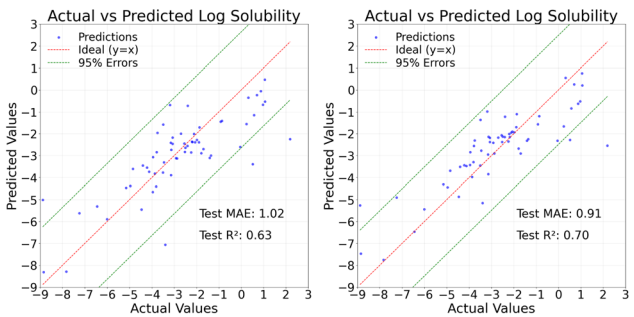

(a) HASolGNN. (b) HASolGNN-LLMs.

Fig. 11 Visualization of solubility prediction errors of HASolGNN *vs.* HASolGNN-LLMs on a small dataset (test set size = 62).

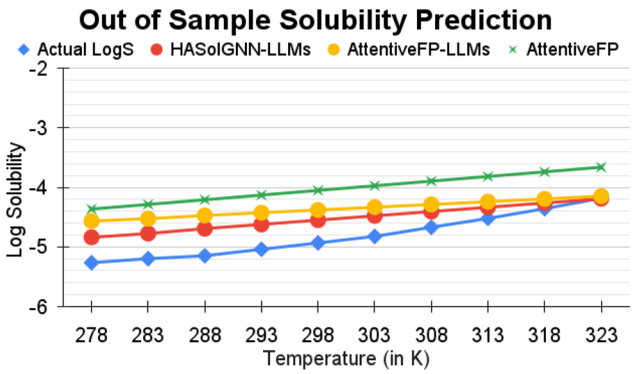

Fig. 12 An example of prediction of the solubility of a solute–solvent pair across varying temperatures (BigSolDB).

Fig. 10: (1) HASolGNN-LLMs consistently achieves lower test MAE (higher test R-squared) compared to HASolGNN as the sample size grows from 1% to 10% of Exp-DB; (2) the error reduction (improvements in R-squared) achieved by HASolGNN-LLMs gradually reduces as the sample size increases; and (3) for both HASolGNN and HASolGNN-LLMs, the errors decrease (R-squared increases) as the sample size grows. The shrinking reduction of errors and improvements of R-squared by HASolGNN-LLMs can be attributed to the higher data availability and quality as more samples are included, which enhances the effectiveness of supervised graph learning. Notably, at the 10% sampling rate, the performance gain (reduction in MAE) achieved by HASolGNN-LLMs is only 0.0114, suggesting that the benefit of the LLM module gradually diminishes. Nonetheless, performance at small data sizes is extremely valuable given the significant cost of obtaining effective experimental data for new classes of systems (Fig. 11).

We next investigate how incorporating the LLM module may help under the inductive learning setting on BigSolDB. This scenario presents challenges due to dataset sparsity, which arises from the limited amount of unique solute–solvent pairs in BigSolDB. Fig. 12 illustrates the performance of HASolGNN-LLMs and Attentive-LLM in predicting solubility of an out-of-sample test solute–solvent pair across varying temperatures.

Table 2 Ablation studies w/o IE, ME, AE, or sum pooling

I: Interaction embedding (IE)	Exp-DB	MolMerger	BigSolDB
HASolGNN w. IE	0.7315	0.7124	0.7408
HASolGNN w/o. IE[1]	0.8394	0.8014	1.0219
HASolGNN w/o. IE w. CA[2]	0.7928	0.7657	0.8263
Improvements over[1]	12.86%	11.11%	27.51%
Improvements over[2]	7.73%	6.96%	10.34%
II: Molecular embedding (ME)	**Exp-DB**	**MolMerger**	**BigSolDB**
HASolGNN w. ME	0.7315	0.7124	0.7408
HASolGNN w/o. ME	0.7560	0.8354	0.8491
Improvements	3.24%	14.73%	12.75%
III: Atom embedding (AE)	**Exp-DB**	**MolMerger**	**BigSolDB**
HASolGNN w. AE	0.7315	0.7124	0.7408
HASolGNN w/o. AE	0.7610	0.7720	0.7601
Improvements	3.89%	7.72%	2.54%
IV: Different pooling	**Exp-DB**	**MolMerger**	**BigSolDB**
HASolGNN w. Average pooling	0.9033	0.7865	1.0214
HASolGNN w. Maximal pooling	0.8570	0.7643	0.8045
Improvements	17.17%	7.29%	8.60%

We observe that incorporating the LLM module to both AttentiveFP and HASolGNN can significantly improve the solubility prediction in the inductive setting.

3.2.2 Robustness of HASolGNN. We evaluate the robustness of HASolGNN against the state-of-the-art method AttentiveFP by randomly sampling the subsets of the Exp-DB dataset, ranging from 20% to 100% of the size of the original Exp-DB dataset. As the size of datasets increases, we observe two major trends from Fig. 13: (1) the test MAE of both HASolGNN and AttentiveFP decreases slightly and (2) HASolGNN consistently outperforms AttentiveFP by maintaining comparable performance gains across all sampling rates. The first trend indicates that the larger datasets enhance the performance as they provide enriched signals. In addition, the performance

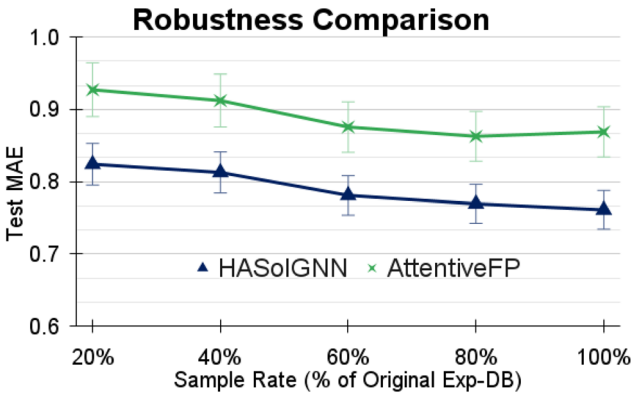

Fig. 13 The robustness of HASolGNN *vs.* AttentiveFP in terms of dataset size (sampled from Exp-DB).

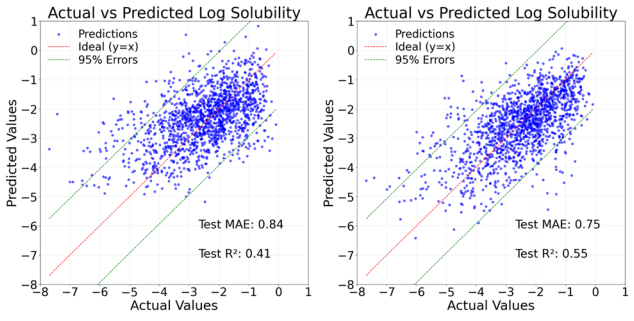

(a) AttentiveFP. (b) HASolGNN.

Fig. 14 Visualization of solubility prediction errors of HASolGNN *vs.* AttentiveFP on MolMerger (completely unseen setting, where both solute and solvent in the test set are unseen during training).

Table 3 Comparison of BigSolDB and BigSolDB v2 in terms of dataset size and test performance

Dataset	Sample size	Unique solutes	Unique solvents	Test MAE (trained on[1])	Test MAE (trained on[2])
BigSolDB[1]	54 273	830	138	0.7408	0.8521
BigSolDB v2[2]	103 944	1448	213	1.0932	0.9275

gains by both HASolGNN and AttentiveFP are relatively modest between 20% and 100%. Even at the 20% sample rate, the dataset contains a relatively large number of solute–solvent pairs, given the large size of Exp-DB. The latter trend demonstrates that HASolGNN consistently delivers robust performance gains over AttentiveFP. The improvements achieved by HASolGNN over AttentiveFP are non-trivial. As shown in Fig. 13, across all sampling rates from 20% to 100%, HASolGNN achieves an average 11.23% reduction in MAE, with performance gains exceeding 10% at every sampling level. These consistent improvements demonstrate the robustness of HASolGNN in capturing solute–solvent interactions across varying data sizes.

3.2.3 Ablation studies. We conduct four sets of ablation studies to evaluate the effectiveness of the key components in HASolGNN: (1) w/o IE block: removing the Interaction-graph Embedding (IE) block from HASolGNN, case one: HASolGNN w/o IE, we replace the IE block by concatenation of both solute embeddings MF_{solute} and solvent embeddings $MF_{solvent}$ with a MLP layer; case two: HASolGNN w/o. IE w. CA, we replace the IE block by computing cross-attention between MF_{solute} and $MF_{solvent}$ and applied on MF_{solute}; (2) w/o ME block: the Molecule Embedding (ME) blocks are removed, leaving only one Atom Embedding (AE) block in both MFGMs (please refer to the HASolGNN framework in Fig. 2); (3) w/o AE block: removing the AE block from HASolGNN (only one ME block left in both MFGMs, please refer to Fig. 2); and (4) w/o sum pooling: replacing all the sum pooling in HASolGNN by either average pooling or maximal pooling.

As illustrated in Table 2, we observe the followings: (1) incorporating the IE Block into HASolGNN reduces the test MAE by an average of 17.16% across all three datasets compared to HASolGNN w/o. IE and an average of 8.34% compared to HASolGNN w/o. IE w. CA; (2) adding the ME block improves test MAE by an average of 10.24% across all datasets; (3) incorporating the AE block into HASolGNN has less impacts on prediction errors compared to IE and ME blocks, reducing the test MAE by 4.72%; and (4) replacing the sum pooling with average pooling increases the test MAE by 23.93% while substituting it with maximal pooling results in an 11.02% increase in test MAE. Our experiments have confirmed the effectiveness of the key components and justify the design choices including the IE block, ME block, AE block, and sum pooling. Together, these components contribute significantly to the improved solubility prediction achieved by HASolGNN.

3.2.4 Generalization to new chemical classes. To evaluate how HASolGNN generalizes to out-of-the-sample test samples, we partitioned the MolMerger dataset such that solutes and solvents in the training, validation, and test sets are mutually exclusive. This split follows a nearly 6 : 2 : 2 ratio, as detailed in Sec. 3.1. Fig. 14 visualizes the solubility prediction errors of HASolGNN compared to AttentiveFP on the completely unseen test dataset of MolMerger. This test presents the most challenging solubility prediction scenario where both solute and solvent graphs are unseen during the model training. The results demonstrate that HASolGNN predictions align more closely with the ideal fit (where predicted values exactly match actual values) in the most challenging case. Specifically, compared to AttentiveFP, HASolGNN (1) achieves a 9.93% lower test MAE and (2) reduces the number of predictions with absolute errors over two (outside the two green lines) by 35.32%.

We observe the larger prediction spread under the "new chemical classes" setting, as shown in Fig. 14, compared to the "pair-unseen" scenario illustrated in Fig. 9. This arises because (1) both solutes and solvents in the test set are unseen during training, forcing the model to extrapolate beyond its learned chemical domain; (2) unlike the "pair-unseen" scenario, where individual solute and solvent embeddings have been learned previously—this case lacks familiar structural or interaction patterns, leading to greater epistemic uncertainty and wider residual variance; (3) the unseen molecules also introduce distribution shifts in molecular features and interaction behaviors, further increasing prediction dispersion. Despite this challenge, HASolGNN maintains lower bias and error than AttentiveFP by leveraging its hierarchical solute–solvent encoding and interaction fusion, which transfer generalizable chemical relations across classes (Table 3).

Case study: trained on BigSolDB and tested on BigSolDB v2. To evaluate the generalizability of HASolGNN, we conduct a case study by applying the HASolGNN model *M*, originally trained on BigSolDB,[15] to BigSolDB v2,[75] the most extensive and up-to-date solubility dataset for organic compounds. Compared to BigSolDB, BigSolDB v2 contains 91.52% more solubility measurements and 74.45% more unique compounds. On this substantially larger dataset, the pre-trained *M* attains a MAE of 1.10 on BigSolDB v2. This is slightly higher than the test MAE of 0.93 achieved by a HASolGNN model newly trained on BigSolDB v2, which is expected given the sheer size and diversity of BigSolDB v2, as well as broader temperature range that is outside the trained model.

4 Conclusion

We have proposed HASolGNN, a novel graph learning framework optimized to effectively exploit multi-level features, and both intra- and inter-molecular interactions for solubility analysis. HASolGNN outperforms all the baseline models, establishing a new benchmark in solubility prediction performance. Notably, HASolGNN outperforms the state-of-the-art

AttentiveFP by further reducing MAE by 15.81%, 11.35%, and 29.59% on the Exp-DB, MolMerger, and BigSolDB dataset, respectively. The superior performance of HASolGNN benefits from its novel and more intricate design compared to previous methods, as verified by our ablation studies. Unlike previous GNN methods for solubility prediction that focus only on atom- and molecule-level interactions and often fail to capture the complex dynamics of solute–solvent interplay, HASolGNN introduces a novel hierarchical encoding framework that models the dissolution process across multiple scales. Attention mechanisms are integrated at each level, atom and bond level (AE block), molecular (ME block), and system-level interaction (IE block), enabling HASolGNN to jointly learn fine-grained structural details and higher order solute–solvent dynamics. Besides, our experiments also demonstrate the robustness of HASolGNN, showing that it generalizes well to new chemical classes and unseen solute–solvent pairs. On the MolMerger split with mutually exclusive solutes and solvents, HASolGNN reduces the amount of large-error (absolute error over two) predictions by 35.52% compared to AttentiveFP. When directly applied to BigSolDB v2 without retraining, the pre-trained model trained by BigSolDB maintains strong performance with a MAE of 1.10, close to 0.93 MAE achieved by retraining. Critically, we have shown that HASolGNN (MAE $\approx$ 0.75 in BigSolDB) approaches the same aleatoric data limit (MAE = 0.5–1 in $\log S$) as identified in previous work, indicating that a further improvement in the accuracy of our models likely requires improved datasets.[28]

We have also introduced a new variant of HASolGNN with the enhancement of LLMs, HASolGNN-LLMs, which integrates a pluggable and fine-tunable LLM module to tackle small-dataset challenges such as data scarcity and biased sampling. To evaluate the effectiveness of HASolGNN-LLMs, we conducted controlled experiments on Exp-DB by randomly sampling subsets ranging from 1% to 10% the size of the Exp-DB dataset. Across all sample sizes, HASolGNN-LLMs consistently achieved lower prediction errors than HASolGNN, confirming the advantage of leveraging LLM-enriched feature space in data-limited regimes. We observe that the smaller the dataset, the larger the performance gains achieved by HASolGNN-LLMs. At the 5% sampling level, the reduction narrows to about 0.03 while at the 1% sampling rate, HASolGNN-LLMs reduces the average MAE by more than 0.08 compared to HASolGNN. In conclusion, our experimental studies have verified that HASolGNN-LLMs yields substantial improvements in solubility prediction and remains robust for out-of-sample test pairs.

Author contributions

Y. F., Y. W., R. F., and M. G. T. designed the experiments and methodologies. M. G. T. supervised the development of the GNN framework and helped perform data curation and analysis. Y. F. conducted the experiments, performed the analysis, and prepared the figures. P. Y. and D. P. conceived the idea and supervised the project. All authors contributed to discussions and jointly authored the manuscript.

Conflicts of interest

There are no conflicts to declare.

Data availability

All datasets, source codes of model and training, running examples, and pre-trained models presented in this paper are available in the HASolGNN GitHub repository (https://github.com/Yangxin666/HASolGNN) and are also publicly available on Zenodo under the DOI https://doi.org/10.5281/zenodo.17848849.

Supplementary information: we provide a proof of the computational complexity of HASolGNN and introduce Para-HASolGNN, a three-level parallel training algorithm to accelerate the training process of HASolGNN. See DOI: https://doi.org/10.1039/d5dd00407a.

Acknowledgements

Y. F., Y. W., and R. F. are supported by the Department of Energy's National Nuclear Security Administration under Award Number(s) DE-NA0004104. D. P., M. G. T., and P. Y. acknowledge the support by the U.S. Department of Energy, Office of Science, Office of Basic Energy Sciences, Heavy Element Chemistry Program under contract KC0302031 E3M2 at Los Alamos National Laboratory (LANL), which is operated by Triad National Security, LLC, for the National Nuclear Security Administration of the U.S. Department of Energy (contract no. 89233218CNA000001). This research used resources of the National Energy Research Scientific Computing Center (NERSC), a Department of Energy Office of Science User Facility using NERSC award BES-ERCAP0023367 and BES-ERCAP0033948.

Notes and references

1 X. Xu, T. Han, J. Huang, A. A. Kruger, A. Kumar and A. Goel, *ACS Appl. Mater. Interfaces*, 2021, **13**, 53375–53387.
2 K. De Jesus, R. Rodriguez, D. Baek, R. Fox, S. Pashikanti and K. Sharma, *J. Mol. Liq.*, 2021, **336**, 116006.
3 C. Long, Z. Jiang, J. Shangguan, T. Qing, P. Zhang and B. Feng, *Chem. Eng. J.*, 2021, **406**, 126848.
4 M. Bouzidi, F. Yahia, S. Ouni, N. B. H. Mohamed, A. S. Alshammari, Z. R. Khan, M. Mohamed, O. A. Alshammari, A. Abdelwahab, A. Bonilla-Petriciolet, et al., *Opt. Mater.*, 2024, 116575.
5 B. Liu, J. Li, W. Yang, X. Zhang, X. Jiang and Y. Bando, *Small*, 2017, **13**, 1701998.
6 P. Shiri, V. Lai, T. Zepel, D. Griffin, J. Reifman, S. Clark, S. Grunert, L. P. Yunker, S. Steiner, H. Situ, et al., *Iscience*, 2021, **24**, xx–yy.
7 N. J. Szymanski, Y. Zeng, H. Huo, C. J. Bartel, H. Kim and G. Ceder, *Mater. Horiz.*, 2021, **8**, 2169–2198.
8 Y. J. Li, K. Wu, Y. Li, Y. Zhang, J. J. Liu and X. Z. Wang, *J. Chem. Eng. Data*, 2018, **63**, 27–38.

9 X. Du, Y. Li, Y.-L. Xia, S.-M. Ai, J. Liang, P. Sang, X.-L. Ji and S.-Q. Liu, *Int. J. Mol. Sci.*, 2016, **17**, 144.
10 R. Qing, S. Hao, E. Smorodina, D. Jin, A. Zalevsky and S. Zhang, *Chem. Rev.*, 2022, **122**, 14085–14179.
11 B. Das, A. T. Baidya, A. T. Mathew, A. K. Yadav and R. Kumar, *Bioorg. Med. Chem.*, 2022, **56**, 116614.
12 A. Jouyban, E. Rahimpour and Z. Karimzadeh, *J. Mol. Liq.*, 2021, **343**, 117587.
13 D. V. Bhalani, B. Nutan, A. Kumar and A. K. Singh Chandel, *Biomedicines*, 2022, **10**, 2055.
14 J. Liu, X. Lei, C. Ji and Y. Pan, *Front. Pharmacol*, 2023, **14**, 1255181.
15 L. Krasnov, S. Mikhaylov, M. Fedorov and S. Sosnin, 2023.
16 J. Chen, S. Zheng, H. Zhao and Y. Yang, *J. Cheminf.*, 2021, **13**, 1–10.
17 S. Lee, M. Lee, K.-W. Gyak, S. D. Kim, M.-J. Kim and K. Min, *ACS Omega*, 2022, **7**, 12268–12277.
18 W. Ahmad, H. Tayara and K. T. Chong, *ACS Omega*, 2023, **8**, 3236–3244.
19 Z. Xiong, D. Wang, X. Liu, F. Zhong, X. Wan, X. Li, Z. Li, X. Luo, K. Chen, H. Jiang, et al., *J. Med. Chem.*, 2019, **63**, 8749–8760.
20 O. Jovic and R. Mouras, *Molecules*, 2023, **29**, 19.
21 D. S. Palmer, N. M. O'Boyle, R. C. Glen and J. B. Mitchell, *J. Chem. Inf. Model.*, 2007, **47**, 150–158.
22 J. McDonagh, T. van Mourik and J. B. Mitchell, *Mol. Inf.*, 2015, **34**, 715–724.
23 A. Jouyban, A. Shayanfar, V. Panahi-Azar, J. Soleymani, B. Yousefi, W. Acree Jr and P. York, *J. Pharm. Sci.*, 2011, **100**, 4368–4382.
24 P. Llompart, C. Minoletti, S. Baybekov, D. Horvath, G. Marcou and A. Varnek, *Sci. Data*, 2024, **11**, 303.
25 P. Ruelle, C. Rey-Mermet, M. Buchmann, H. Nam-Tran, U. W. Kesselring and P. Huyskens, *Pharm. Res.*, 1991, **8**, 840–850.
26 H. R. Amedi, A. Baghban and M. A. Ahmadi, *J. Mol. Liq.*, 2016, **216**, 411–422.
27 E. M. Tosca, R. Bartolucci and P. Magni, *Pharmaceutics*, 2021, **13**, 1101.
28 L. Attia, J. W. Burns, P. S. Doyle and W. H. Green, *Nat. Commun.*, 2025, **16**, 7497.
29 W. Ahmad, H. Tayara, H. Shim and K. T. Chong, *Int. J. Mol. Sci.*, 2024, **25**, 715.
30 G. Panapitiya, M. Girard, A. Hollas, J. Sepulveda, V. Murugesan, W. Wang and E. Saldanha, *ACS Omega*, 2022, **7**, 15695–15710.
31 S. Lee, H. Park, C. Choi, W. Kim, K. K. Kim, Y.-K. Han, J. Kang, C.-J. Kang and Y. Son, *Sci. Rep.*, 2023, **13**, 957.
32 T. Zheng, J. B. Mitchell and S. Dobson, *ACS Omega*, 2024, **9**, 35209–35222.
33 N. Saquer, R. Iqbal, J. D. Ellis and K. Yoshimatsu, *Digital Discovery*, 2024, **3**, 602–609.
34 R. J. Leenhouts, N. Morgan, E. Al Ibrahim, W. H. Green and F. H. Vermeire, *Chem. Eng. J.*, 2025, **513**, 162232.
35 H. Jung, C. D. Stubbs, S. Kumar, R. Pérez-Soto, S.-m. Song, Y. Kim and S. Kim, *Digital Discovery*, 2025, **4**, 1492–1504.
36 Z. Wu, S. Pan, F. Chen, G. Long, C. Zhang and S. Y. Philip, *IEEE Transact. Neural Networks Learn. Syst.*, 2020, **32**, 4–24.
37 T. N. Kipf and M. Welling, *arXiv*, 2016, preprint, arXiv:1609.02907, DOI: 10.48550/arXiv.1609.02907.
38 W. Hamilton, Z. Ying and J. Leskovec, *Adv. Neural Inf. Process. Syst.*, 2017, **30**, xx–yy.
39 P. Velickovic, G. Cucurull, A. Casanova, A. Romero, P. Lio, Y. Bengio, et al., *stat*, 2017, **1050**, 10–48550.
40 K. Xu, W. Hu, J. Leskovec and S. Jegelka, *arXiv*, 2018, preprint, arXiv:1810.00826, DOI: 10.48550/arXiv.1810.00826.
41 A. Lusci, G. Pollastri and P. Baldi, *J. Chem. Inf. Model.*, 2013, **53**, 1563–1575.
42 C. Merkwirth and T. Lengauer, *J. Chem. Inf. Model.*, 2005, **45**, 1159–1168.
43 M. Withnall, E. Lindelöf, O. Engkvist and H. Chen, *J. Cheminf.*, 2020, **12**, 1.
44 F. Scarselli, M. Gori, A. C. Tsoi, M. Hagenbuchner and G. Monfardini, *IEEE Trans. Neural Network.*, 2008, **20**, 61–80.
45 E. N. Feinberg, D. Sur, Z. Wu, B. E. Husic, H. Mai, Y. Li, S. Sun, J. Yang, B. Ramsundar and V. S. Pande, *ACS Cent. Sci.*, 2018, **4**, 1520–1530.
46 D. K. Duvenaud, D. Maclaurin, J. Iparraguirre, R. Bombarell, T. Hirzel, A. Aspuru-Guzik and R. P. Adams, *Adv. Neural Inf. Process. Syst.*, 2015, **28**, xx–yy.
47 C. W. Coley, R. Barzilay, W. H. Green, T. S. Jaakkola and K. F. Jensen, *J. Chem. Inf. Model.*, 2017, **57**, 1757–1772.
48 X. Wang, Z. Li, M. Jiang, S. Wang, S. Zhang and Z. Wei, *J. Chem. Inf. Model.*, 2019, **59**, 3817–3828.
49 S. Ryu, J. Lim, S. H. Hong and W. Y. Kim, *arXiv*, 2018, preprint, arXiv:1805.10988, DOI: 10.48550/arXiv.1805.10988.
50 Z. Hao, C. Lu, Z. Huang, H. Wang, Z. Hu, Q. Liu, E. Chen and C. Lee, *Proceedings of the 26th ACM SIGKDD international conference on knowledge discovery & data mining*, 2020, pp. 731–752.
51 K. Yang, K. Swanson, W. Jin, C. Coley, P. Eiden, H. Gao, A. Guzman-Perez, T. Hopper, B. Kelley, M. Mathea, et al., *J. Chem. Inf. Model.*, 2019, **59**, 3370–3388.
52 Z. Chen, L. Chen, S. Villar and J. Bruna, *Adv. Neural Inf. Process. Syst.*, 2020, **33**, 10383–10395.
53 A. Mayr, G. Klambauer, T. Unterthiner, M. Steijaert, J. K. Wegner, H. Ceulemans, D.-A. Clevert and S. Hochreiter, *Chem. Sci.*, 2018, **9**, 5441–5451.
54 M. Meng, Z. Wei, Z. Li, M. Jiang and Y. Bian, *IEEE 10th International Conference on Software Engineering and Service Science (ICSESS)*, 2019, pp. 263–266.
55 N. Sukumar and J. Pask, *Int. J. Numer. Methods Eng.*, 2009, **77**, 1121–1138.
56 K. Zhou, Y. Dong, K. Wang, W. S. Lee, B. Hooi, H. Xu and J. Feng, *Proceedings of the 30th ACM International Conference on Information & Knowledge Management*, 2021, pp. 2728–2737.
57 J. Wu, J. Wang, Z. Wu, S. Zhang, Y. Deng, Y. Kang, D. Cao, C.-Y. Hsieh and T. Hou, *J. Chem. Inf. Model.*, 2022, **62**, 5975–5987.
58 J. Achiam, S. Adler, S. Agarwal, L. Ahmad, I. Akkaya, F. L. Aleman, D. Almeida, J. Altenschmidt, S. Altman,

S. Anadkat et al., *arXiv*, 2023, preprint, arXiv:2303.08774, DOI: 10.48550/arXiv.2303.08774.
59 A. Grattafiori, A. Dubey, A. Jauhri, A. Pandey, A. Kadian, A. Al-Dahle, A. Letman, A. Mathur, A. Schelten, A. Vaughan et al., *arXiv*, 2024, preprint, arXiv:2407.21783, DOI: 10.48550/arXiv.2407.21783.
60 Full, 2025, https://github.com/Yangxin666/HASolGNN/blob/main/HASolGNN_full.pdf.
61 W. L. Jorgensen and E. M. Duffy, *Adv. Drug Deliv. Rev.*, 2002, **54**, 355–366.
62 I. Beltagy, K. Lo and A. Cohan, *arXiv*, 2019, preprint, arXiv:1903.10676, DOI: 10.48550/arXiv.1903.10676.
63 Y. Gu, R. Tinn, H. Cheng, M. Lucas, N. Usuyama, X. Liu, T. Naumann, J. Gao and H. Poon, *ACM Trans. Comput. Healthc.*, 2021, **3**, 1–23.
64 R. Miao, Y. Yang, Y. Ma, X. Juan, H. Xue, J. Tang, Y. Wang and X. Wang, *Inf. Sci.*, 2022, **613**, 667–681.
65 Y. Kim, H. Jung, S. Kumar, R. S. Paton and S. Kim, *Chem. Sci.*, 2024, **15**, 923–939.
66 V. Ramani and T. Karmakar, *J. Chem. Theory Comput.*, 2024, **20**, 6549–6558.
67 S. Boobier, D. R. Hose, A. J. Blacker and B. N. Nguyen, *Nat. Commun.*, 2020, **11**, 5753.
68 J. S. Delaney, *J. Chem. Inf. Comput. Sci.*, 2004, **44**, 1000–1005.
69 Q. Chen, Y. Zhang, P. Gao and J. Zhang, *Artif. Intell. Chem.*, 2023, **1**, 100010.
70 T. Xie and J. C. Grossman, *Phys. Rev. Lett.*, 2018, **120**, 145301.
71 Y. Qiu, J. Chen, K. Xie, R. Gu, Z. Qi and Z. Song, *Chem. Eng. Sci.*, 2024, **300**, 120559.
72 A. Yang, S. Sun, H. Mi, W. Wang, J. Liu and Z. Y. Kong, *Ind. Eng. Chem. Res.*, 2024, **63**, 8293–8305.
73 H.-C. Liao, Y.-H. Lin, C.-H. Peng and Y.-P. Li, *ACS Eng. Au*, 2025, **5**, 530–539.
74 F. J. Pontes, G. Amorim, P. P. Balestrassi, A. Paiva and J. R. Ferreira, *Neurocomputing*, 2016, **186**, 22–34.
75 L. Krasnov, D. Malikov, M. Kiseleva, S. Tatarin, S. Sosnin and S. Bezzubov, *Sci. Data*, 2025, **12**, 1236.